Acta Materialia

Effect of Temperature on the Devitrification Kinetics of NiTi Films

Michael J. Vestel[1], David S. Grummon[2], Ronald Gronsky[3], Albert P. Pisano[4]

[1]*Lab for Ultra Small Technologies Engineering & Research (LUSTER), Engineering Division, Berkeley Lab, Berkeley, CA, 94720*

[2]*Chemical Engineering & Materials Science, Michigan State University, East Lansing, MI 48824*

[3]*Materials Science & Engineering, University of California, Berkeley, CA 94720*

[4]*Mechanical Engineering, University of California, Berkeley, CA 94720*

Abstract

The effect of isothermal devitrification temperature on the reaction kinetics and the microstructure of freestanding NiTi films have been studied using differential scanning calorimetry (DSC) and transmission electron microscopy (TEM). The minimum temperature for complete crystallization of amorphous sputtered films was found to be 400°C, and analysis of the nucleation kinetics yielded Avrami exponents between 2 and 3 for all films. Crystalline grains always nucleated first at the surface, grew laterally until impingement, then grew inward to form columnar grains. Surface roughness delayed the onset of surface nucleation. In very smooth surfaced films, multiple DSC exotherms heralded repeated nucleation of new wide, flat grains within the film interior. This secondary microstructure exhibited different kinetics than the columnar grains, and Avrami exponents consistent with a continuous nucleation mode.

Corresponding author:
Michael J. Vestel, Lab for Ultra Small Technologies Engineering & Research (LUSTER), Engineering Division, Berkeley Lab, Berkeley, CA, 94720, Fax (510) 486-6596, Email mvestel@lbl.gov

Keywords:
1. Synthesis and Processing: Thin Films
2. Characterization: Transmission Electron Microscopy (TEM)
3. Material Type: Shape Memory Alloys (SMA), Thin Films
4. Properties and Phenomena: Crystallization
5. Theory and Modeling: Kinetics

1. Introduction

Crystalline Ni-Ti films are known to possess superelastic (SE) properties and display a robust shape memory effect (SME) [1-8] applicable where resilient mechanical response is essential, or where thermal actuation or sensing is desired, particularly for photolithogtraphically machined microelectromechanical systems (MEMS). One such application of increasing importance in the biomedical field is the fabrication of micro-needles [9-18] for transdermal or subdermal fluid transport, including the integration of micro-needles with silicon structures [19] such as bio-MEMS assemblies. The direct deposition of crystalline Ni-Ti alloys onto silicon is, however, complicated by mismatched thermal expansion coefficients [20,21] that induce large tensile film stresses on cooling, often causing catastrophic delamination of films thicker than 5 to 7 microns [3]. This obstacle can be overcome by depositing at low temperature to obtain an amorphous phase, and subsequently crystallizing (also known as "devitrifying" because it follows from a "glassy" phase) the product after releasing it from its substrate. Since lithographic micromachining of amorphous films with HF etchants yields more precise etch profiles and smoother surfaces [22,23], the crystallization (devitrification) treatment should follow all micromachining operations. And since the displacive transformation associated with the SME is strongly dependent upon the microstructure [7] of the crystallized product, the devitrification reaction must be carefully controlled. These issues motivated the present study, which seeks to understand the kinetics and nucleation modes associated with the devitrification reaction in a model NiTi system.

2. Background

Moberly, *et al.* [1] confirmed that amorphous NiTi films crystallized to the ordered B2 (CsCl) phase, as opposed to disordered bcc, and measured a crystallization enthalpy of 21.6 J/g at 490ºC in DSC experiments. When crystallization occurred under electron bombardment in a transmission electron microscope (TEM), spheroidal grains nucleated inside a 300 nm thick foil, and new grains were observed to nucleate as others grew prior to impingement. An activation energy of 385±96 kJ/mol was estimated for the crystallite growth rate based on TEM video recordings made between 597 and 540ºC. Gisser, *et al*, [24] found that Ti-Ni thin films deposited onto (100) silicon substrates at elevated temperature (460ºC) were crystalline and had (110) sheet texture. This same study showed that deposition temperatures could be lowered to 350ºC after nucleation of the crystalline phase at >460ºC. It was later shown by Hou *et al*. [2] that the (110) sheet texture disappeared at deposition temperatures above 425ºC.

Chen, *et al*. [25] compared the activation energies determined by Kissinger's method for crystallization of sputtered amorphous $Ti_{49.93}Ni_{50.07}$ and $Ti_{49.96}Ni_{40.09}Cu_{9.95}$ films. These authors reported amorphous films containing Cu were thermally less stable than the nearly equiatomic NiTi film, with crystalline activation energies of 388kJ/mol at an isochronal crystallization temperature (T_x) of 497°C and 416kJ/mol at T_x = 482°C for a 10 K/min DSC heating rate. Chang and Grummon [8] showed that T_x at 10 K/min decreased with increasing Ti content, from 490ºC for $Ni_{52.6}Ti_{47.4}$, to 475ºC for $Ni_{49}Ti_{51}$, and observed a systematic increase of T_x with heating rate. These authors also estimated that the activation energy for crystallization ranged from 385 kJ/mol for $Ni_{49}Ti_{51}$ to 501 kJ/mol for $Ni_{52.6}Ti_{47.4}$. They furthermore characterized the crystallization reaction as fully "polymorphic," concluding that a supersaturated solid solution was readily obtained in sputtered films, unlike the case for melt-solidified alloys. Grummon and Zhang [26] showed that isothermal crystallization of TiNi on (100)-Si produced a transient increase in tensile film stress of approximately 180 MPa. The time for this stress to develop was analyzed as a function of the annealing temperature to give an activation energy for growth of the crystalline phase of 477 kJ/mol.

Recently, the sensitivity of microstructure to crystallization temperature was demonstrated in [6]. $Ni_{48.2}Ti_{51.8}$ films, annealed at 472ºC for 1 hour, developed fine GP-zone-like precipitates that very effectively increased the

critical resolved shear stress for slip. Annealing at 414ºC for 2 h maximized the strengthening effect at the expense of incomplete crystallization.

The present work was undertaken to clarify details of the crystallization reaction in free-standing sputtered TiNi films, and to establish critical kinetic parameters governing isothermal nucleation of the crystalline phase between 390ºC and 450ºC, below the nominal isochronal crystallization temperature. Such low temperature post processing crystallization anneals would be favorable for post CMOS modular integration. We also address aspects of microstructural development that could have important implications for subsequent displacive transformation behavior, by experiments on partially crystallized films.

3. Experimental Procedures

Near-equiatomic NiTi films were deposited on stainless steel (SS) and silicon substrates by DC diode magnetron sputtering. The NiTi films deposited on SS were sputtered from 75 mm diameter $Ti_{52}Ni_{48}$ alloy targets under 3.0 mTorr of argon gas at 100°C and cathode power of 250 W. Ti-rich targets were used to compensate for Ti depletion during the sputtering process. The resulting 22 micron thick near-equiatomic amorphous films were brittle, with a dull metallic luster, and a pronounced surface roughness inherited from the substrate finish. Large pieces were easily peeled from the substrate. A 13 micron amorphous film was then sputter-deposited on a five-inch (100)-silicon substrate using the same deposition conditions. This film was tough and very smooth with a bright metallic luster. The metallized wafer was diced and the films delaminated by cyclic immersion in liquid nitrogen and 100°C water. Adhesion was sufficiently moderate to support delamination via crack propagation through the silicon substrates. X-ray diffraction confirmed that the films were amorphous.

All films were isothermally or isochronally annealed in a power-compensated TA Instruments 2920 DSC under a nitrogen atmosphere in aluminum container pans. For isothermal anneals, the furnace and reference pans were first equilibrated to the desired temperature, then the furnace lid was removed and the sample placed rapidly into the furnace as data recording initiated. This approach allowed minimal overshoot and fastest temperature equilibration. Isochronal calorimetry for determination of the dynamic crystallization temperature was performed using a protocol similar to that of Scott [27] and others [28-30] at a constant rate of 10K/min. The onset of crystallization at this heating rate for a 22μm thick amorphous film released from a SS substrate was marked by a single distinct 33J/g exotherm at 451ºC, in general agreement with previously published results [30-32]. This temperature was taken to be the dynamic crystallization temperature, T_x. Additional free-standing film specimens, detached from both Si and SS substrates, were then isothermally crystallized in the calorimeter at progressively lower temperatures until no crystallization exotherm could be observed.

The DSC data were analyzed to determine the mode of crystallization from the shape of the isothermal crystallization peaks using the Johnson-Mehl-Avrami (JMA) model [33-35]. Avrami [36] proposed that the general relation

$$X(t) = 1 - \exp\left[-k(t-\tau)^n\right] \qquad (1)$$

should be applicable when the nucleation rate is a decreasing function of time and approaches an asymptote. Here, $X(t)$ is the phase fraction transformed (crystallized) at time t, k is a rate constant and τ is an incubation period for establishment of a steady-state population of crystalline nucleii. The time exponent n reflects the mode and dimensionality of the process; for the two-dimensional regime applicable to thin films the limiting cases are a constant nucleation rate (continuous nucleation) or a constant growth rate (site saturation). Continuous and site-saturation nucleation modes in thin films are therefore predicted to produce Avrami exponents, n, of three (3) and two (2) respectively [36].

It has been shown [37-41] that $X(t)$ corresponds to the fractional area under the exothermal crystallization peak in a DSC thermogram, $A(t)/A_{total}$, integrated from the onset of transformation at time τ, to some later time t. After determining the incubation time τ by inspection, linearizing Eq. 1 and plotting $\ln(-\ln[1-X(t)])$ vs. $\ln(t-\tau)$, the time exponent, n, is extracted from the slope of the resulting line. Integrating the peak areas using the TA Universal Analysis DSC software package with appropriately interpolated baselines produces sigmoidal transformation curves like the one shown in Fig. 1. These curves establish the time for 50% crystallization ($t_{50\%}$) and the incubation period. Crystalline fractions for a minimum of 100 different times were calculated. Though the plots are not shown, activation energies were estimated from an Arrhenius relationship of the form $t_{50\%} = t_0 \exp(Q/RT)$, where t_0 is a constant, Q is the activation energy, and R is the molar gas constant. The slope of $\ln(t_{50\%})$ vs $1/RT$ therefore yields Q. The calorimetry data were additionally used to design isothermal annealing experiments for production of rough and smooth film specimens with carefully controlled partial crystallization. Partially and fully transformed films were then analyzed to establish interphase interfacial morphologies at various crystallization temperatures below the nominal T_x.

3.1 Transmission Electron Microscopy

Transmission electron microscopy samples, transverse to the plane of the film, were prepared by the wedge method [42]. Multiple ion milling steps were performed using a Fischione Instruments model 3000 ion mill with two guns oriented 12º above and 12° below the plane of the rotating TEM foil surface. During rotation, the guns were activated only during the interval with they came within ± 30º of normal to the film-substrate interface. Ion milling continued for 60 to120 minutes at 5kV and between 4.0 and 5.5mA. A final cleanup step was performed at 4kV and 4.0mA using a stationary 6º tilt for one full rotation of the sample.

Samples were examined in JEOL JEM3010, Philips CM200 and JEOL JEM200CX transmission electron microscopes at the National Center for Electron Microscopy (NCEM) [43]. Low temperature observations were made in the liquid nitrogen cooled double-tilt stage of the CM200, while heating experiments were performed in the double tilt stage of the JEM 200CX.

4. Results and Discussion

4.1 NiTi Films Released from Stainless Steel Substrates

Amorphous NiTi films released from stainless steel substrates were isothermally crystallized in the calorimeter at temperatures between 440 and 390ºC for times as long as 600 minutes. The lowest crystallization temperature at which an exothermic peak could be easily discerned was 420ºC, as shown in Fig. 2. As the annealing temperature was lowered from 440ºC to 420ºC, the incubation time increased and the devitrification curve broadened as expected [39,40,44,45]. Annealing at 400ºC for 400 minutes and 390ºC for 600 minutes produced no identifiable crystallization exotherm.

Figure 3 shows JMA plots of $\ln(-\ln[1-X(t)])$ vs. $\ln(t-\tau)$ using the data from Fig. 1 and the annealing temperatures in Fig. 2. Between X=0.01 and X=0.85, the graphs are linear with a correlation better than R^2=0.9993. Incubation times and Avrami exponents determined from this data are summarized in Table 1.

Table 1: Values of $\boldsymbol{\tau}$, $t_{50\%}$ and $\boldsymbol{n}$ for isothermally annealed films released from SS

T (°C)	τ (min)	$t_{50\%}$(min)	n

420	29	37	2.6
430	11	17	2.6
435	5	10.7	2.5
440	4	6.84	2.3

The activation energy based on analysis of times for 50% crystallization at the various temperatures was found to be 347 kJ/mol (83kcal/mol), within the range of previously reported values for NiTi, as well as other metallic glass systems [1,8,25-27,37,46-48]. The method for the determination of the activation energy for crystallization appears to be valid for these films because of the accurate fit of the data to a straight line. Furthermore, TEM of transverse foils confirmed that the crystalline phase nucleated entirely at the free surfaces, and no evidence of additional nucleation in the interior was found. Consequently the isothermal DSC peaks represent single surface-crystallization events that allow accurate determination of the activation energy for crystallization.

Transmission electron micrographs of the specimen annealed at 430°C reveal that the crystalline phase nucleated at both free surfaces. One such image of a film annealed for 25 minutes (Fig. 4) shows a 4.7 micron deep crystalline zone at one of the two free surfaces where nucleation occurred. Growth of the surface-nucleated phase continued until lateral (in-plane) impingement, after which a columnar growth mode persisted in the direction of the film-plane normal. A higher magnification image of the crystalline/amorphous interface (Fig. 4 inset) shows that the interphase interface is faceted, but all grains appear to be growing into the amorphous phase at nearly the same rate. The typical grain diameter in the plane of the film is approximately one micron, similar to values reported in the literature for NiTi films when devitrified from the amorphous state [4,49,50].

Analysis of the two films annealed at 430ºC, one for 80 minutes and one for 25 minutes, confirmed that the relative area under the DSC exotherm accurately corresponds to the relative amount crystallized. Because the freestanding foil was 22.4 μm thick, two crystalline layers (each 4.7 μm thick) represent 42% crystallization. The time for 42% crystallization determined from Fig. 1, using the relative area model, is $\tau+t_{42\%}=11+15=26$ minutes, corresponding well with the observed 25 minute crystallization time measured at 430ºC.

At the highest annealing temperature, 450°C, the Avrami exponent was determined to be n=2.3, which increased to 2.6 as the temperature was lowered, both values within the band between n=2 and n=3 expected for thin foils [36]. However, the micrographs reveal that the devitrification reaction nucleated on the surface, representing a site saturation mode as the available surface sites were depleted.

Table 2: Kinetic Parameters for films released from Silicon

Annealing Temperature (°C)	Enthalpy of Crystallization (J/g)	First Peak				Second Peak			
		τ (min)	$t_{50\%}$(min)	*Q (KJ/mol)*	*n*	τ (min)	$t_{50\%}$ (min)	*Q (KJ/mol)*	*n*
420	17	18.4	8	~352	2.8	37	28.6	~406	2.9
425	17	6.4	7	~352	2.4	32	14.5	~406	3.1
430	18	5.7	3.3		*	20.7	10.5		*
440	23	1.6	10.1	~435	2.5	-	-		-
450	22	1.1	3.7	~435	2.1	-	-		-

* Peaks could not be separated with sufficient accuracy.

4.2 NiTi Films Released from Silicon Substrates

Crystallization exotherms for film specimens released from silicon are shown in Fig. 5. As was the case for films released from SS substrates, annealing at temperatures below 420°C did not produce a detectable exotherm for holding times up to 600 minutes. Specimens annealed at 420ºC and 425ºC showed two crystallization peaks that could be separated sufficiently well to permit JMA analysis on each peak (plots not shown). JMA plots of the films annealed at 450ºC and 440ºC, which showed single crystallization peaks, are shown in Fig. 3. The results are tabulated in Table 2 (which additionally indicates the observed transient times τ, the 50% crystallization times, and the calculated activation energies).

The isothermal DSC peaks (Fig. 5) showed that 17-23 J/g of heat evolved from the films annealed between 420ºC and 450ºC. For films annealed at 430, 425 and 420ºC, summing the contribution from the two crystallization peaks gave values of 17 to 18 J/g for the crystallization enthalpy, somewhat lower than the 22-23 J/g for films crystallized at 450ºC and 440ºC. The latter data may contain errors attributable to the very short incubation time for annealing at higher temperature which may have caused inaccuracy in establishing the correct baseline at the beginning of the exotherm.

The activation energies of the two separate peaks (Table 2) were similar to the values observed for films released from SS and other amorphous alloys [37]. The activation energies of the two types of grains appear to be similar, but only two data points were used to determine Q.

Multiple peaks in the DSC spectra of the smooth surface specimens (NiTi on silicon) are evident at all temperatures in Fig. 5. These results, combined with the different Avrami exponents for the first and second peaks, suggest multiple nucleation and growth regimes with distinct kinetic parameters evidenced by the increasing interval between peaks at low temperatures.

Confirmation of this behavior is provided in the TEM images of transverse foils made from partially-crystallized films, showing the full through-thickness structure. For samples grown on rough-surfaced substrates that showed only a single DSC crystallization peak, the partially-crystallized NiTi films exhibited three strata: two outer zones of surface-nucleated columnar grains, and an inner zone of remnant, perfectly homogenous amorphous metal. The interior interfaces appeared generally like that shown in Fig. 4. For samples grown on smooth-surfaced substrates that showed multiple crystallization exotherms, the partially-crystallized NiTi films exhibited five strata (see Fig. 8). These include: two outer zones of surface-nucleated columnar grains, two inner homogenous amorphous alloy zones, and a fifth stratum of wide, flat grains that nucleated in the film interior, independent of any surface nucleation events. The more complex stratified microstructures are shown in Fig. 7, crystallized at 425ºC for 120 min. Both Figs. 6 and 7 show surface-nucleated columnar grains at the top that have impinged on larger, plate-shaped grains at the bottom. The bright field (BF) and dark field (DF) TEM images (Fig. 7) show a 3.4 μm wide plate shaped grain in the center of the image, separated by arrowed high angle grain boundaries from contiguous plate-shaped grains. Other TEM observations illustrate that these grains could be as wide as 5 μm, and they are all at least 3 μm thick. The central 1/3 of all films grown on smooth substrates were made up of these plate shaped grains. The two DSC peaks shown in Fig. 5 therefore correspond to the two morphologies, columnar and plate, seen in these micrographs.

The lowest devitrification temperature at which films were observed to be fully crystalline was 400°C, and examination of a film annealed at 390ºC for 600 minutes (not included) exhibited only surface-nucleated columnar grains and a remnant amorphous stratum in the center of the film. The first of the two DSC peaks for the low-temperature anneals therefore corresponds to the growth of surface-nucleated columnar grains.

Table 2 furthermore shows that the second peaks are associated with Avrami exponents close to 3, indicating that plate-shaped grains nucleated in a continuous mode, since such nucleation at grain interior sites is appropriately described by the Avrami analysis [36]. The shallow plate morphology indicates that lateral

growth velocity is substantially higher than the plane-normal growth rate. It is unlikely that preexisting crystalline embryos or clusters were frozen into the amorphous NiTi films during deposition because of the clear documentation of an incubation period in the DCS analyses, which increased with a corresponding decrease in crystallization temperature.

5. Conclusions

Low temperature, post processing crystallization anneals have been shown to successfully devitrify freestanding NiTi films after release from their sputtering substrates. Such low annealing temperatures would be favorable for their CMOS compatibility and thus are important to the applications of MEMS structures. This study shows that devitrification in a reasonable length of time requires annealing temperatures of at least 400^{o}C. The crystalline phase nucleates first at free surfaces, with incubation times increasing with decreasing temperature, and activation energies between 347 and 435 kJ/mol. Roughened surfaces appear to lengthen the nucleation phase. Nucleation occurs almost simultaneously at both free surfaces and leads to impingement of columnar grains near the center of the film when crystallization is complete. Amorphous-crystalline interfaces are found to be nominally flat. Initial rapid lateral growth of surface nucleated crystallites leads to early impingement of the grains within the plane of the film, after which continued growth normal to the surface proceeds at a substantially slower rate. In-plane grain profiles are equiaxed, with a typical grain diameter of 1 micrometer, and are elongated in the film growth direction. Little dependence of grain size on annealing temperature is observed. Even when surface nucleation takes place rapidly, additional bulk nucleation events are found to occur, producing stratified regions of crystalline material with relatively shallow, wide grains, in sharp contrast to the high aspect ratio and orientation of the surface-nucleated grains. These grains nucleate in the interior of the film, independent of any surface nucleated columnar grains, leading to multi-directional laminar microstructures that can be expected to show altered martensitic transformation behavior.

Acknowledgments

The films used in this study were prepared by Thomas LaGrange and Wangyang Ni at Michigan State University. The authors thank Professor Nitash P. Balsara and Hany Eitouni, Department of Chemistry, UC Berkeley, for use of the DSC, and Dr. Eric Stach, Dr. Tamara Radetic and Chris Nelson, at the National Center for Electron Microscopy for assistance with TEM.

Figure Captions

Figure 1: Typical DSC curve for an isothermal anneal. Film was released from its SS substrate and annealed at 430ºC. Also shown is the X vs. t sigmoidal type relationship illustrating the incubation time, τ (11 min.), and the time for 50% crystallization (17 min.) used to determine the activation energy for crystallization. The sigmoidal X vs. t data appears in Avrami plots, Fig. 3.

Figure 2: Isothermal DSC plot of 22μm amorphous equiatomic NiTi film released from a SS substrate showing broadening of crystallization peaks and increase in incubation times as the crystallization temperature is lowered. Films annealed at 400°C and 390°C show no distinguishable exotherms.

Figure 3: Johnson-Mehl-Avrami plots for free-standing NiTi films released from a SS substrate and crystallized at the indicated temperatures. The Avrami exponent increases from 2.3 to 2.6 as the annealing temperature is lowered. Also shown are the secondary DSC peaks for two films released from silicon.

Figure 4: TEM image of one of two surfaces showing microstructure resulting from surface nucleation of columnar grains (top) growing into remnant amorphous phase (bottom). Sample was crystallized at 430ºC and quenched in liquid nitrogen after 25 min. Inset close-up of interface shows grain size is approximately 1μm.

Figure 5: Isothermal anneals of freestanding NiTi released from a silicon substrate. The lowest devitrification temperature shown in this figure is 420ºC, but films were annealed to as low as 390ºC and still showed signs of partial crystallization. Note that devitrification is delayed and the peak broadens as the annealing temperature is lowered and diffusion becomes more sluggish. Double crystallization peaks imply different parts of the film crystallized at different times.

Figure 6: TEM cross-sectional micrograph of NiTi released from silicon after crystallizing at 420ºC for 200 minutes. Columnar grains are at the top of the image, which nucleated at the surface of the film and consumed the amorphous phase. Plate-shaped grains are shown at the bottom of the image.

Figure 7: TEM cross-section of film annealed at 425ºC for 120 minutes, shown in BF (a) and DF (b), modes. The DF image was produced using one of the martensite reflections in the inset diffraction pattern to highlight one of the plate-shaped grains in the lower half of the image.

Figure 8: TEM cross-section of film annealed at 440ºC for only 12 minutes. A 1.1 μm thick amorphous layer (diffraction pattern inset) separates columnar grains at the top of the image from the plate shaped grains at the bottom of the image. The image on the right side shows a close-up of the amorphous region sandwiched by the two grains.

Please NOTE: Figures are a little smaller than the requested print size. The downloaded EPS figures are accurate in dimensions.

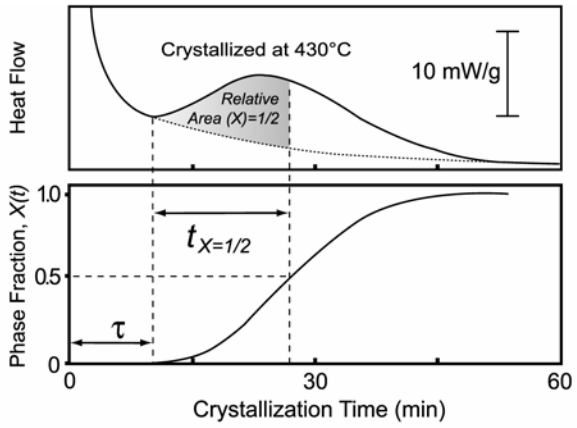

Fig. 1

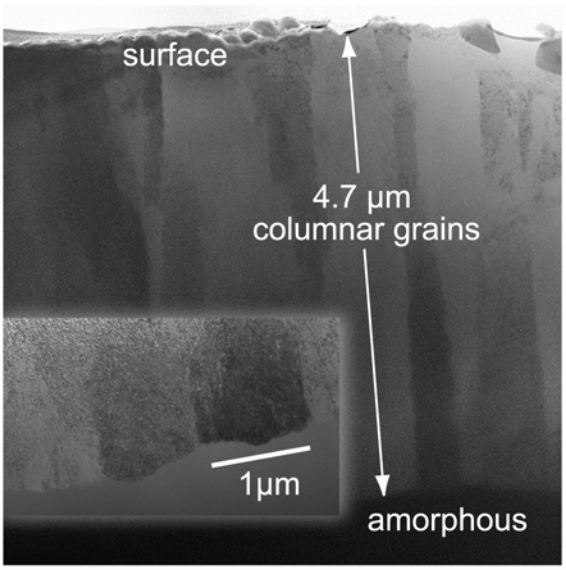

Fig. 4

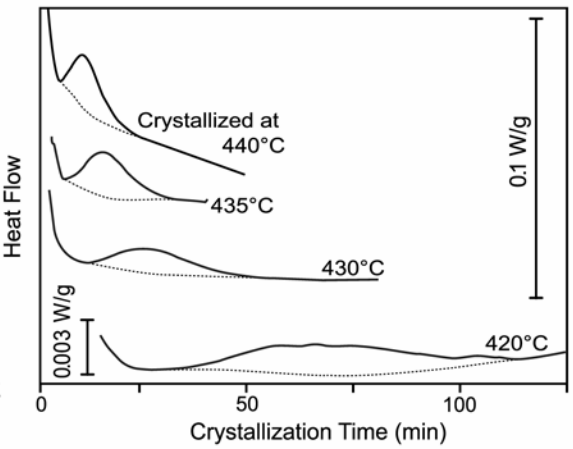

Fig. 2

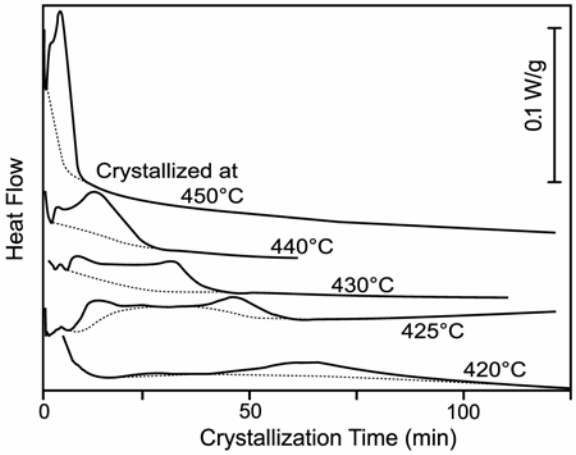

Fig. 5

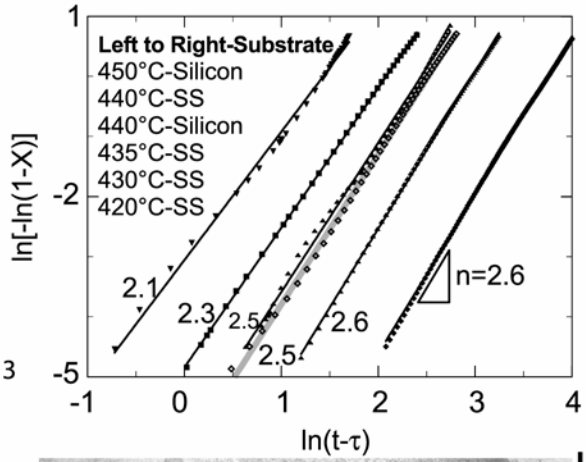

Fig. 3

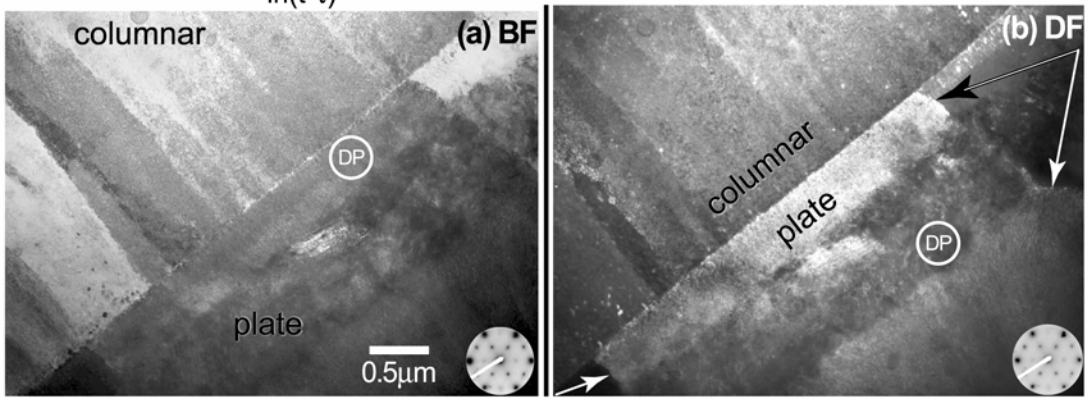

Fig. 7

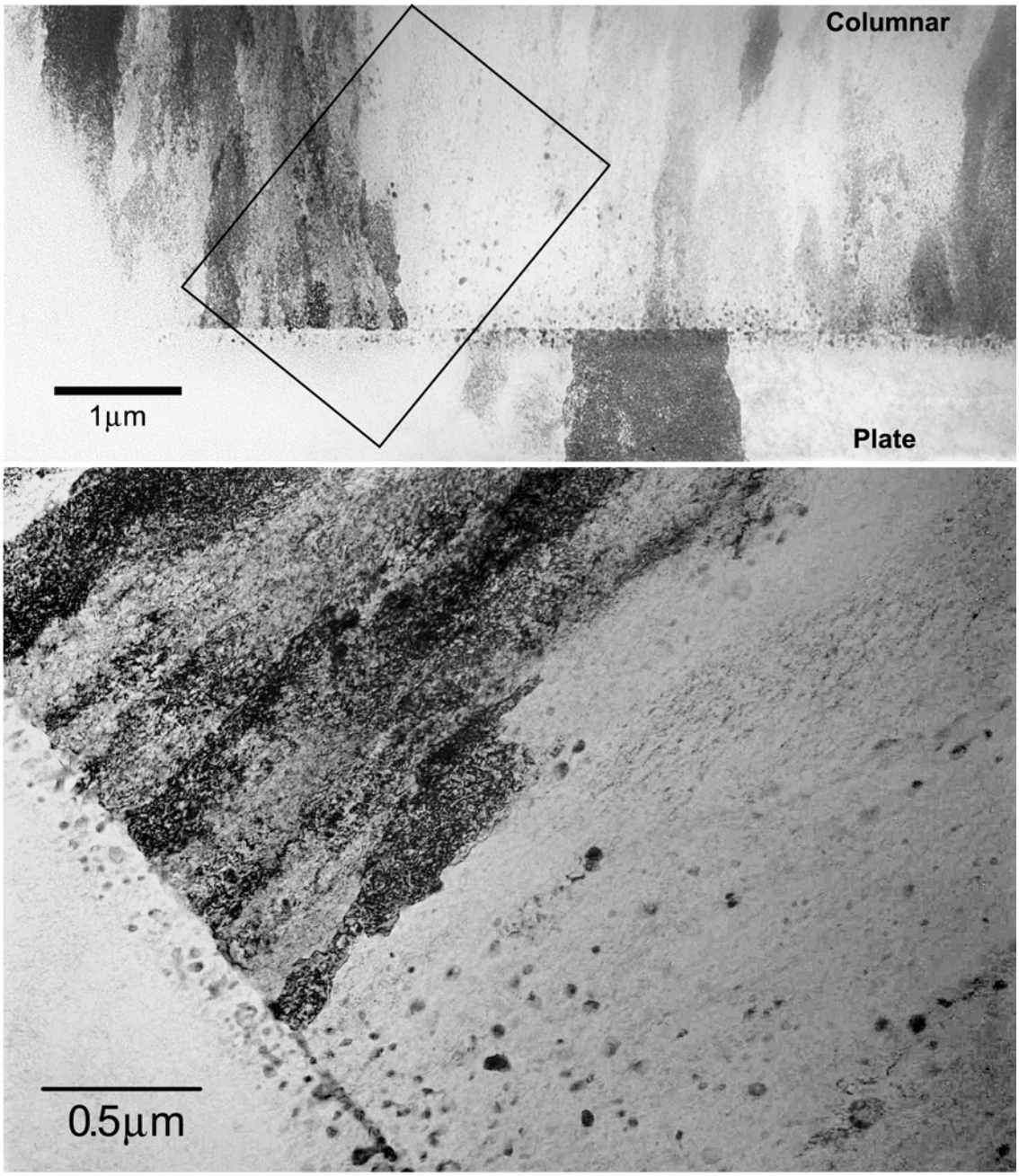
Columnar
1μm
Plate
0.5μm

Fig. 6

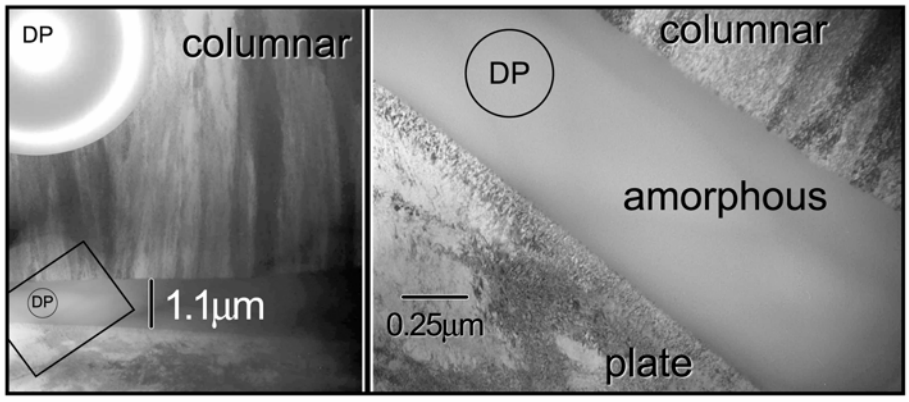
DP
columnar
DP
columnar
amorphous
1.1μm
0.25μm
plate

Fig. 8

References

[1] Moberly WJ, Busch JD, Johnson AD, and Berkson MH. *In-Situ Hvem of Crystallization of Amorphous Tini Thin Films.* In: Chen M, Thompson MO, Schwarz RB, and Libera M, editors. Phase Transformation Kinetics in Thin Films Symposium, vol. 230. Anaheim, CA, USA: Mater. Res. Soc, 1991. p.85-90.

[2] Hou L and Grummon DS. Scripta Metall. et Mater. 1995;**33**:989-995.

[3] Grummon DS, LaGrange T, and Zhang J. *Processing and Deployment of Sputtered Thin Films of NiTi and Nitix Alloys for Biomedical and Mems Applications.* In: Russel SM and Pelton A, editors. SMST-2000: Proceedings of the International Conference on Shape Memory and Superelastic Technologies, Asilomar, CA, USA: 2000.

[4] Kajiwara S, Ogawa K, Kikuchi T, Matsunaga T, and Miyazaki S. Phil. Mag. Let. 1996;**74**:395-404.

[5] Miyazaki S, Nomura K, Ishida A, and Kajiwara S. *Recent Developments in Sputter-Deposited Ti-Ni-Base Shape Memory Alloy Thin Films.* In: IVth European Symposium on Martensitic Transformations, vol. 7 (C5). Enschede, Netherlands: Editions de Physique, 1997. p.275-80.

[6] Kajiwara S, Kikuchi T, Ogawa K, Matsunaga T, and Miyazaki S. Philosophical Magazine Letters 1996;**74**:137-44.

[7] Otsuka K and Wayman CM. *Shape Memory Materials*. Cambridge: Cambridge University Press, 1998.

[8] Chang L and Grummon DS. Phil. Mag. A 1997;**76**:191-219.

[9] Najafi K and Wise KD. IEEE J. Sol. State Cir. 1986;**21**:1035-44.

[10] Chen J and Wise KD. *A Multichannel Neural Probe for Selective Chemical Delivery at the Cellular Level.* In: Solid-State Sensor and Actuator Workshop, Hilton Head Island, SC, USA: 1994. p.256-259.

[11] Lin L and Pisano AP. J. MEMS 1999;**8**:78-84.

[12] Talbot NH and Pisano AP. *Polymolding: Two Wafer Polysilicon Micromolding of Closed-Flow Passages for Microneedles and Microfluidic Devices.* In: Solid-State Sensor and Actuator Workshop, Hilton Head Island, SC, USA: 1998. p.265-8.

[13] Brazzle J, Bartholomeusz D, Davies R, Andrade J, van Wagenen RA, and Frazier AB. *Active Microneedles with Integrated Functionality.* In: Solid-State Sensor and Actuator Workshop, Hilton Head Island, SC, USA: 2000. p.199-202.

[14] Papautsky I, Brazzle J, Swerdlow H, and Frazier AB. J. MEMS 1998;**7**:267-73.

[15] Papautsky I, Frazier AB, and Swerdlow H. *A Low-Temperature Ic-Compatible Process for Fabricating Surface-Micromachined Metallic Microchannels.* In: Tenth Annual International Workshop on MEMS, Nagoya, Japan: IEEE, 1997. p.317-22.

[16] Brazzle JD, Papautsky I, and Frazier AB. *Fluid-Coupled Hollow Metallic Micromachined Needle Arrays.* In: Microfluidic Devices and Systems, vol. 3515. Santa Clara, CA, USA: SPIE-Int. Soc. Opt. Eng, 1998. p.116-24.

[17] Papautsky I, Brazzle J, Ameel T, and Bruno Frazier A. *Laminar Fluid Behavior in Microchannels Using Micropolar Fluid Theory.* In: IEEE Eleventh Annual International Workshop on MEMS, vol. A73. Heidelberg, Germany: Elsevier, 1998. p.101-8.

[18] Henry S, McAllister DV, Allen MG, and Prausnitz MR. *Micromachined Needles for the Transdermal Delivery of Drugs.* In: Eleventh Annual International Workshop on MEMS, Heidelberg, Germany: IEEE, 1998. p.494-8.

[19] Franke AE, *Polycrystalline Silicon-Germanium Films for Integrated Microsystems*, Ph.D. Thesis, Electrical Engineering and Computer Sciences, University of California at Berkeley, 2000.

[20] Haji L, Joubert P, Guendouz M, Duhamel N, and Loisel B. *Substrate Effects on the Kinetics of Solid Phase Crystallization in α-Si.* In: Chen M, Thompson MO, Schwarz RB, and Libera M, editors. Phase Transformation Kinetics in Thin Films Symposium, vol. 230. Anaheim, CA, USA: Mater. Res. Soc, 1991. p.177-82.

[21] Kim JJ, Moine P, and Stevenson DA. Scripta Metall. 1986;**20**:243-8.

[22] Makino E, Mitsuya T, and Shibata T. Sensors and Actuators A 2000;**79**:251-9.

[23] Guifu D, Aibin Y, Xiaolin Z, Dong X, Bingchu C, and Tianhui S. *Patterning of Nickel-Titanium SMA Films with Chemical Etching by a Novel Multicomponent Etchant.* In: Device and Process Technologies for MEMS and Microelectronics, vol. 3892. Gold Coast, Australia: SPIE-Int. Soc. Opt. Eng, 1999. p.340-5.

[24] Gisser KRC, Busch JD, Johnson AD, and Ellis AB. App. Phys. Let. 1992;**61**:1632-4.

[25] Chen JZ and Wu SK. J. Non-Crys. Sol. 2001;**288**:159-65.

[26] Grummon DS and Zhang J. Phys. Stat. Sol. A 2001;**186**:17-39.

[27] Scott MG and Ramachandrarao P. Mater. Sci. Eng. 1977;**29**:137-144.

[28] Marshall AF, Walmsley RG, and Stevenson DA. Mater. Sci. Eng. 1984;**63**:215-227.

[29] Makifuchi Y, Terunuma Y, and Nagumo M. Mater. Sci. Eng. 1997;**A226-228**:312-316.

[30] Busch JD, Johnson AD, Lee CH, and Stevenson DA. J. App. Phys. 1990;**68**:6224-6228.

[31] Chang L and Grummon DS. Phil. Mag. A 1997;**76**:163-89.

[32] Kajiwara S, Ogawa K, Kikuchi T, Matsunaga T, and Miyazaki S. *Unique Crystallization Process in Sputter-Deposited Ti-Ni Shape Memory Films.* In: Ninth International Conference on Rapidly Quenched and Metastable Materials, vol. A226-228. Bratislava, Slovakia: Elsevier, 1996. p.53-5.

[33] Avrami M. J. Chem. Phys. 1941;**9**:177-84.

[34] Avrami M. J. Chem. Phys. 1940;**8**:212-24.

[35] Avrami M. J. Chem. Phys. 1939;**7**:1103-12.

[36] Christian JW. *The Theory of Transformations in Metals and Alloys: An Advanced Textbook in Physical Metallurgy*. 2nd ed. Oxford, New York: Pergamon Press, 1981.

[37] Scott MG. J. Mat. Sci. 1978;**13**:291-6.

[38] Scott MG and Ramachandrarao P. Mat. Sci. Eng. 1977;**29**:137-44.

[39] Greer AL. *Crystal Nucleation and Growth in Metallic Liquids and Glasses.* In: P.Haasen and Jaffee RI, editors. Acta-Scripta metallurgica Proceedings Series, vol. 3. New York: Pergamon Press, 1985. p.94-107.

[40] Luborsky FE. *Amorphous Metallic Alloys*. London; Boston: Butterworths, 1983.

[41] Fujita H, Komatsu M, Sakata T, and Fujita N. Mat. Trans., JIM 1996;**37**:1350-5.

[42] Phelps JM. Microscopy and Microanalysis 1998;**4**:128-32.

[43] http://ncem.lbl.gov/frames/center.htm.

[44] Shimomura K, Shingu PH, and Ozaki R. J. Mat. Sci. 1980;**15**:1175-82.

[45] Cahn RW and Haasen P. *Physical Metallurgy*. 3rd ed. New York: Elsevier Science Publisher, 1983.

[46] Scott MG. *Thermal Stability and Crystallisation of Metallic Glasses.* In: Rapidly Quenched Metals III, Brighton, UK: Metals Soc, 1978. p.198-213.

[47] Scott MG and Watanabe T. *Crystallisation of Some Metallic Glasses.* In: Spring Residential Conference, York, UK: Inst. Metallurgists, 1979. p.36-8.

[48] Thompson CV, Greer AL, and Spaepen F. Acta Metall. 1983;**31**:1883-94.

[49] Miyazaki S and Ishida A. Mater. Sci. Eng. 1999;**A273-275**:106-133.

[50] Chang L and Grummon DS. *Orthorhombic Martensite, Intermetallic Precipitates and Retained Austenite in Ti-Rich Ti(Ni+Cu) Sputtered Thin Films.* In: Materials Research Society Symposium, vol. 246. 1992. p.141-146.